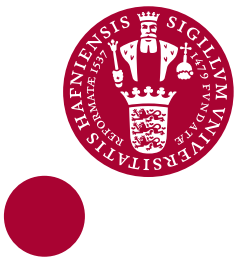

Non-redundant ISGF3 Components Promote NK Cell Survival in an Auto-regulatory Manner during Viral Infection

Geary, Clair D.; Krishna, Chirag; Lau, Colleen M.; Adams, Nicholas M.; Gearty, Sofia V.; Pritykin, Yuri; Thomsen, Allan R.; Leslie, Christina S.; Sun, Joseph C.

Published in:
Cell Reports

DOI:
10.1016/j.celrep.2018.07.060

Publication date:
2018

Document version
Publisher's PDF, also known as Version of record

Cell Reports

Report

Non-redundant ISGF3 Components Promote NK Cell Survival in an Auto-regulatory Manner during Viral Infection

Graphical Abstract

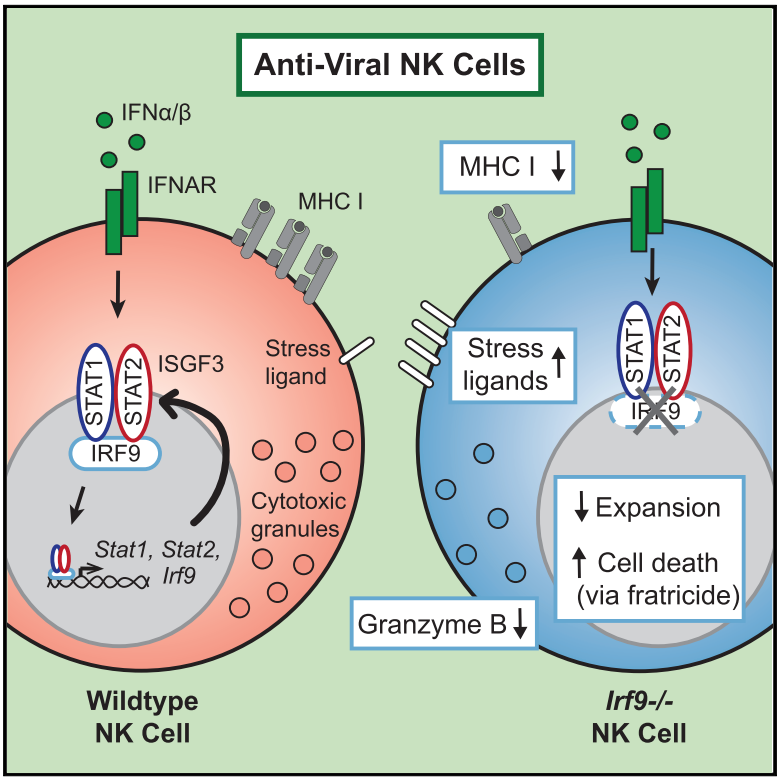

Highlights

- IFN-α induces ISGF3 components in NK cells by an auto-regulatory feedforward loop
- Some IFNAR-dependent transcripts in MCMV-activated NK cells are STAT1 independent
- ISGF3 components are non-redundant in promoting MCMV-driven NK cell expansion
- IRF9 shields NK cells from apoptosis by regulating cell surface molecule expression

Authors

Clair D. Geary, Chirag Krishna, Colleen M. Lau, ..., Allan R. Thomsen, Christina S. Leslie, Joseph C. Sun

Correspondence

sunj@mskcc.org

In Brief

Using RNA-seq and ChIP-seq, Geary et al. investigate the impacts of type I interferon on NK cells during MCMV infection and demonstrate crucial and non-redundant roles for STAT1, STAT2, and IRF9 in promoting cytotoxicity and survival of antiviral NK cells.

Geary et al., 2018, Cell Reports *24*, 1949–1957
August 21, 2018
https://doi.org/10.1016/j.celrep.2018.07.060

CellPress

Cell Reports
Report

Non-redundant ISGF3 Components Promote NK Cell Survival in an Auto-regulatory Manner during Viral Infection

Clair D. Geary,[1] Chirag Krishna,[2] Colleen M. Lau,[1] Nicholas M. Adams,[1,3] Sofia V. Gearty,[1] Yuri Pritykin,[2] Allan R. Thomsen,[4] Christina S. Leslie,[2] and Joseph C. Sun[1,3,5,6,*]
[1]Immunology Program, Memorial Sloan Kettering Cancer Center, New York, NY 10065, USA
[2]Computational and Systems Biology Program, Memorial Sloan Kettering Cancer Center, New York, NY 10065, USA
[3]Louis V. Gerstner, Jr. Graduate School of Biomedical Sciences, Memorial Sloan Kettering Cancer Center, New York, NY 10065, USA
[4]Department of Immunology and Microbiology, University of Copenhagen, Copenhagen, Denmark
[5]Department of Immunology and Microbial Pathogenesis, Weill Cornell Medical College, New York, NY 10065, USA
[6]Lead Contact
*Correspondence: sunj@mskcc.org
https://doi.org/10.1016/j.celrep.2018.07.060

SUMMARY

Natural killer (NK) cells are innate lymphocytes that possess adaptive features, including antigen-specific clonal expansion and long-lived memory responses. Although previous work demonstrated that type I interferon (IFN) signaling is crucial for NK cell expansion and memory cell formation following mouse cytomegalovirus (MCMV) infection, the global transcriptional mechanisms underlying type I IFN-mediated responses remained to be determined. Here, we demonstrate that among the suite of transcripts induced in activated NK cells, IFN-α is necessary and sufficient to promote expression of its downstream transcription factors STAT1, STAT2, and IRF9, via an auto-regulatory, feedforward loop. Similar to STAT1 deficiency, we show that STAT2- or IRF9-deficient NK cells are defective in their ability to expand following MCMV infection, in part because of diminished survival rather than an inability to proliferate. Thus, our findings demonstrate that individual ISGF3 components are crucial cell-autonomous and non-redundant regulators of the NK cell response to viral infection.

INTRODUCTION

Natural killer (NK) cells are innate lymphocytes that are critical for tumor immunosurveillance and control of herpesvirus infections. NK cell activation is determined by the balance of germline-encoded inhibitory receptors, which recognize major histocompatibility complex (MHC) class I (i.e., "self"), and activating receptors that recognize stressed or infected cells, often in the context of diminished MHC class I (i.e., "missing self") (Lanier, 2008). Upon activation, NK cells rapidly proliferate and release pro-inflammatory cytokines such as IFN-γ and cytotoxic molecules (granzyme B) to lyse transformed or infected target cells (Sun and Lanier, 2011). Although they have traditionally been classified as part of the innate immune system, NK cells are now appreciated to share many features with adaptive lymphocytes, including clonal expansion, longevity, and robust recall responses (Geary and Sun, 2017). One of the most well characterized models of "adaptive" NK cell responses occurs during mouse cytomegalovirus (MCMV) infection. The MCMV-encoded glycoprotein m157 is specifically recognized by the Ly49H receptor expressed on a subset of NK cells in C57BL/6 mice, and receptor-ligand engagement drives rapid NK cell proliferation and effector functions that provide resistance to MCMV (Arase et al., 2002; Brown et al., 2001; Daniels et al., 2001; Dokun et al., 2001; Smith et al., 2002). Following their rapid expansion, virus-specific NK cell effectors contract to form a long-lived pool of memory cells that exhibit enhanced effector functions upon secondary challenge (Sun et al., 2009).

Previous studies have demonstrated that pro-inflammatory cytokine signals, particularly IL-12 and type I interferon (IFN), are crucial for NK cell expansion and memory formation (Madera et al., 2016; Sun et al., 2012). Canonical type I IFN signaling requires TYK2 and JAK1-mediated phosphorylation of STAT1 and STAT2, which then form a heterotrimer with IRF9. This complex, termed ISGF3, translocates to the nucleus, where it binds to IFN-stimulated response elements (ISRE) to promote expression of hundreds of IFN-stimulated genes (ISGs) encoding proteins with antiviral functions (Ivashkiv and Donlin, 2014). It is thought that specificity for the ISRE sequence is provided by IRF9, while additional DNA contacts with STAT1 and STAT2 stabilize the interaction, and STAT2 provides the transcriptional activation domain (Bluyssen and Levy, 1997; Levy et al., 1989; Qureshi et al., 1995; Veals et al., 1993; Wesoly et al., 2007). However, there is increasing evidence that alternative complexes, containing unphosphorylated STATs or different combinations of STATs with or without IRF9, also form in response to type I IFN stimulation and may contribute to the pleiotropic biological effects of IFNs (reviewed in Fink and Grandvaux, 2013; Majoros et al., 2017). The biological importance of these alternative pathways has been demonstrated by studies showing that *Stat2*$^{-/-}$ or *Irf9*$^{-/-}$ mice were more resistant to certain viral infections

than *Stat1*$^{-/-}$ mice (Hofer et al., 2012; Perry et al., 2011) and that STAT1-independent transcription of some ISGs can be driven by STAT2 or IRF9 (Luker et al., 2001; Perry et al., 2011). Thus, we sought to better understand the global transcriptional mechanisms underlying type I IFN-mediated responses of NK cells during viral infection and whether these pathways are directly controlled by canonical ISGF3 signaling.

RESULTS AND DISCUSSION

Type I IFN Signaling in NK Cells Induces Auto-regulation of ISGF3 Components

To investigate the genes induced by type I IFNs in NK cells, we performed comparative transcriptome analysis by RNA-sequencing (RNA-seq) on purified NK cells that were stimulated with IFN-α or left unstimulated (media alone). The vast majority of transcriptional changes were induced by IFN stimulation, and the most highly induced genes included many canonical ISGs, such as *Ifit3*, *Rsad2*, and *Isg15* (Figure 1A). Among the genes significantly induced by IFN-α in NK cells, chromatin immunoprecipitation sequencing (ChIP-seq) demonstrated that 32% were bound by STAT1. Interestingly, the most highly differentially expressed genes were not preferentially STAT1 bound (Figure 1B). Among the top STAT1-bound, IFN-α-induced transcription factors were several genes known to be important for the NK cell response to MCMV, such as *Runx3* (Rapp et al., 2017) and *Tbx21* (Madera et al., 2018), as well as all three ISGF3 components (Figure 1C). Analysis of the individual *Stat1*, *Stat2*, and *Irf9* loci confirmed that NK cells exposed to IFN-α significantly induced transcription of these genes (Figure 1D). Furthermore, STAT1 targeted the promoters of all three ISGF3 components (Figure 1E). Thus, we propose that STAT1 (and other ISGF3 components) may operate in an auto-regulatory manner in NK cells during viral infection.

NK Cells Demonstrate IFN-Induced, but STAT1-Independent, Transcriptional Changes during Viral Infection

To determine if all genes induced during type I IFN exposure were dependent on STAT1 signaling for their expression *in vivo*, we performed RNA-seq on wild-type (WT), *Ifnar1*$^{-/-}$, and *Stat1*$^{-/-}$ Ly49H^{+} NK cells from MCMV-infected and uninfected mixed bone marrow chimeric mice (mBMCs) (Figure 2A). We observed 872 differentially expressed genes between WT and *Ifnar1*$^{-/-}$ NK cells (Figure 2B) and 838 differentially expressed genes between WT and *Stat1*$^{-/-}$ NK cells (Figure 2C) at day 1.5 post-infection (PI). Many of the most significant changes were canonical ISGs (e.g., *Irf7*, *Rtp4*, *Mx1*) that were induced *ex vivo* and common between both knockouts. Interestingly, the majority of differentially expressed genes did not overlap with our list of genes induced by IFN-α *ex vivo*. Importantly, we found that after MCMV infection, expression of all three ISGF3 components was upregulated in WT Ly49H^{+} NK cells, but this increase was almost completely abolished in the absence of STAT1 (Figure 2D) or the type I IFN receptor (Figure S1A). These findings are consistent with the auto-regulatory mechanism proposed above and also suggest that ISGF3 components operate in a feedforward manner to promote their own transcription.

Although the transcriptional profile of IFNAR1- and STAT1-deficient NK cells appeared similar at the global level, direct comparison of genes revealed that fewer than 60% of the differentially expressed transcripts were common to both knockouts relative to WT NK cells (Figures 2E and S1B–S1E). The dysregulated genes unique to *Stat1*$^{-/-}$ NK cells could be due to downstream influences of other cytokine signaling pathways that have been proposed to induce phosphorylation of STAT1 (e.g., IFN-γ or IL-21); however, the transcriptional changes unique to *Ifnar1*$^{-/-}$ NK cells suggest that non-canonical type I IFN signaling pathways may be active in NK cells during viral infection.

Individual ISGF3 Components Promote Clonal Expansion of Antiviral NK Cells in a Cell-Autonomous and Non-redundant Manner

This noncongruent transcriptomic profile of *Ifnar1*$^{-/-}$ versus *Stat1*$^{-/-}$ NK cells led us to hypothesize that IRF9, and potentially STAT2, may also play important, non-redundant roles in the response of NK cells to MCMV infection. Because both *Ifnar1*$^{-/-}$ and *Stat1*$^{-/-}$ mice are highly susceptible to MCMV (Gil et al., 2001), we determined whether IRF9 is also required for host control of MCMV infection. We challenged WT and *Irf9*$^{-/-}$ mice with MCMV and found that *Irf9*$^{-/-}$ mice were unable to control the infection, resulting in higher viral titers in the blood (Figure S2A) and early death (Figure S2B).

To more directly interrogate the importance of IRF9 and STAT2 in NK cells, we investigated whether any effector functions of NK cells were abrogated in the absence of these factors. During MCMV infection, activated Ly49H^{+} NK cells proliferate to expand the pool of effector cells (Dokun et al., 2001; Sun and Lanier, 2011). To test the role of IRF9 in the expansion of MCMV-specific NK cells, we co-transferred equal numbers of WT (CD45.1) and *Irf9*$^{-/-}$ (CD45.2) Ly49H^{+}KLRG1^{lo} NK cells into Ly49H-deficient recipients, and following MCMV infection, we tracked the expansion of the transferred Ly49H^{+} NK cells (Figure 3A). In contrast to WT NK cells, which underwent robust expansion, IRF9-deficient NK cells expanded modestly and represented a smaller proportion of the effector and memory NK cell pools (Figures 3B and 3C). STAT2-deficient NK cells showed a similar defect in expansion and contribution to the memory cell pool after MCMV infection (Figures 3D and 3E). Together, these findings demonstrate a non-redundant requirement for all ISGF3 components in promoting NK cell expansion following viral infection.

As has been previously reported for *Ifnar1*$^{-/-}$ mice (Guan et al., 2014; Mizutani et al., 2012), we observed minor defects in NK cell development in the global absence of IRF9 and STAT2 (Figures S3A–S3C; data not shown). To confirm that the expansion defects we observed were due to cell-intrinsic roles for IRF9 and STAT2 during MCMV infection, we generated mBMC by reconstituting irradiated mice with bone marrow from *Irf9*$^{-/-}$ or *Stat2*$^{-/-}$ and WT mice. In this setting, both IRF9- and STAT2-deficient NK cells repopulated the mice with similar efficiency to WT NK cells (Figure S3D; data not shown), and the knockout cells that arose were phenotypically indistinguishable from WT NK cells (Figure S3E; data not shown), suggesting that the developmental defects observed in NK cells

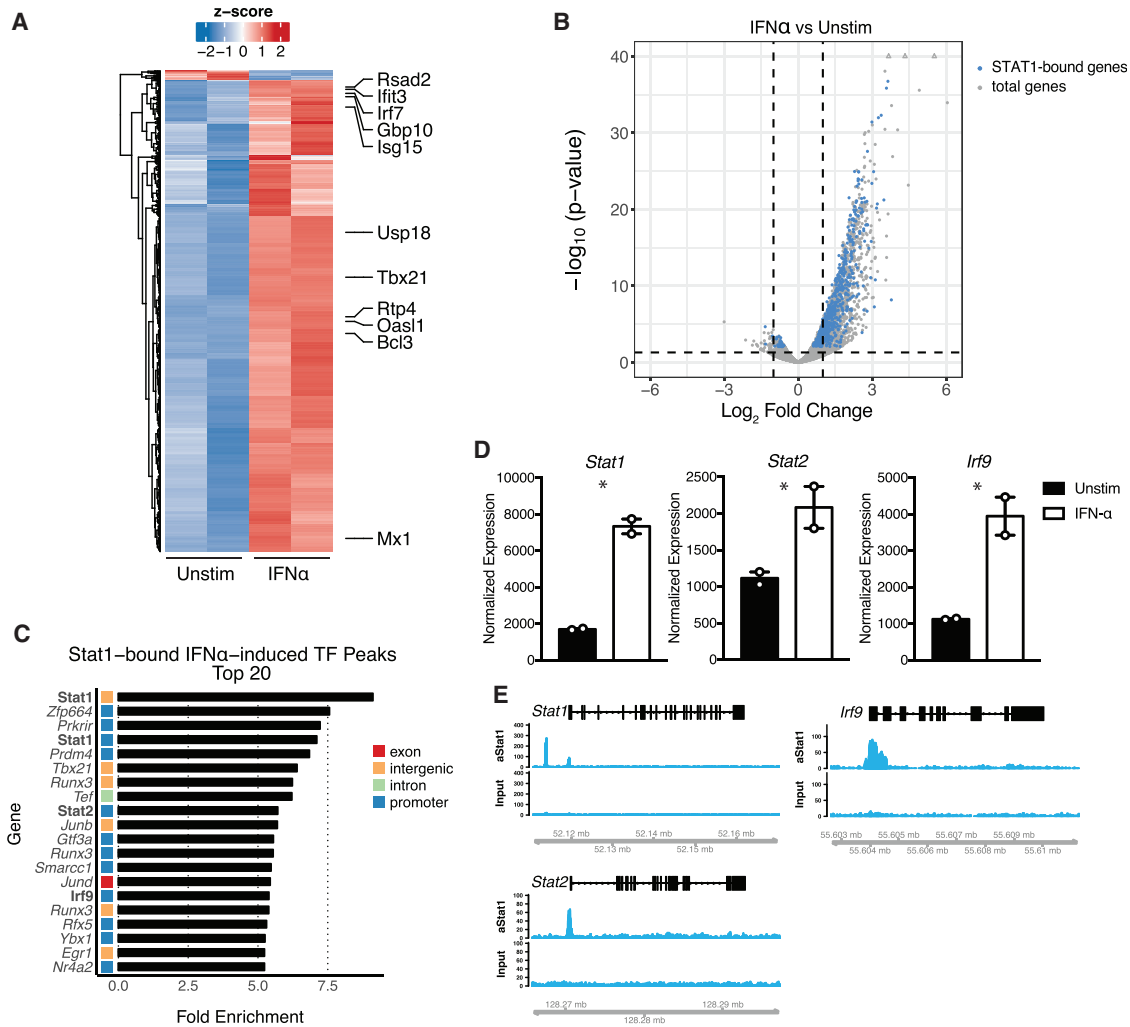

Figure 1. The NK Cell Interferome Reveals Auto-regulation of ISGF3 Components

Splenic NK cells were sort purified and cultured overnight with IFN-α and assayed using RNA-seq and aSTAT1 ChIP-seq. Cells cultured in media alone served as controls for RNA-seq.

(A) Heatmap depicting row-normalized $\log_2$-transformed counts of differentially expressed genes with absolute $\log_2$fold change > 1 and false discovery rate - adjusted p value (FDR) < 0.05 calculated using DESeq2. Genes of interest are labeled.

(B) Volcano plot of RNA-seq data from *ex vivo* stimulated NK cells. Blue dots show differentially expressed (FDR < 0.05) genes bound by STAT1 as determined by ChIP-seq. Horizontal line indicates p = 0.05, and vertical lines show absolute $\log_2$ fold change = 1.

(C) Bar graph depicts fold enrichment of STAT1 binding over input calculated by MACS2. Shown are the top 20 peaks ranked by fold enrichment that are associated with differentially expressed transcription factors as determined by RNA-seq.

(D) Normalized counts of *Stat1*, *Stat2*, and *Irf9* in splenic NK cells unstimulated or cultured overnight with IFN-α assessed using RNA-seq. Symbols represent biological replicates, and error bars show SEM (*p < 0.05).

(E) Representative gene tracks from STAT1 ChIP-seq showing counts on y axis and genomic coordinates on x axis. RNA-seq is two biological replicates. ChIP-seq is two independent experiments of 20–25 pooled mice per experiment.

directly isolated from the *Irf9*$^{-/-}$ or *Stat2*$^{-/-}$ mice were cell extrinsic. When WT and IRF9- or STAT2-deficient cells were adoptively transferred from mBMC into Ly49H-deficient mice, we observed a similar expansion defect in knockout NK cells following MCMV infection (data not shown).

A major function of NK cells during viral infection is to produce pro-inflammatory cytokines such as IFN-γ, in addition to mediating cytotoxicity. In uninfected mice, WT and *Irf9*$^{-/-}$ NK cells showed comparable IFN-γ production and degranulation after *ex vivo* stimulation (Figure S3F; data not shown) and killed m157-expressing target cells similarly (Figure S3G), suggesting that IRF9 does not play a critical role in the acquisition of NK cell effector functions during development. However, during MCMV infection, *Irf9*$^{-/-}$ NK cells failed to upregulate granzyme B to the same extent as WT cells (Figure 3F), although they expressed similar levels of IFN-γ (Figure 3G) and activation markers (Figures 3H and 3I). Thus, defects in expansion and expression of cytolytic molecules by *Irf9*$^{-/-}$ NK cells likely

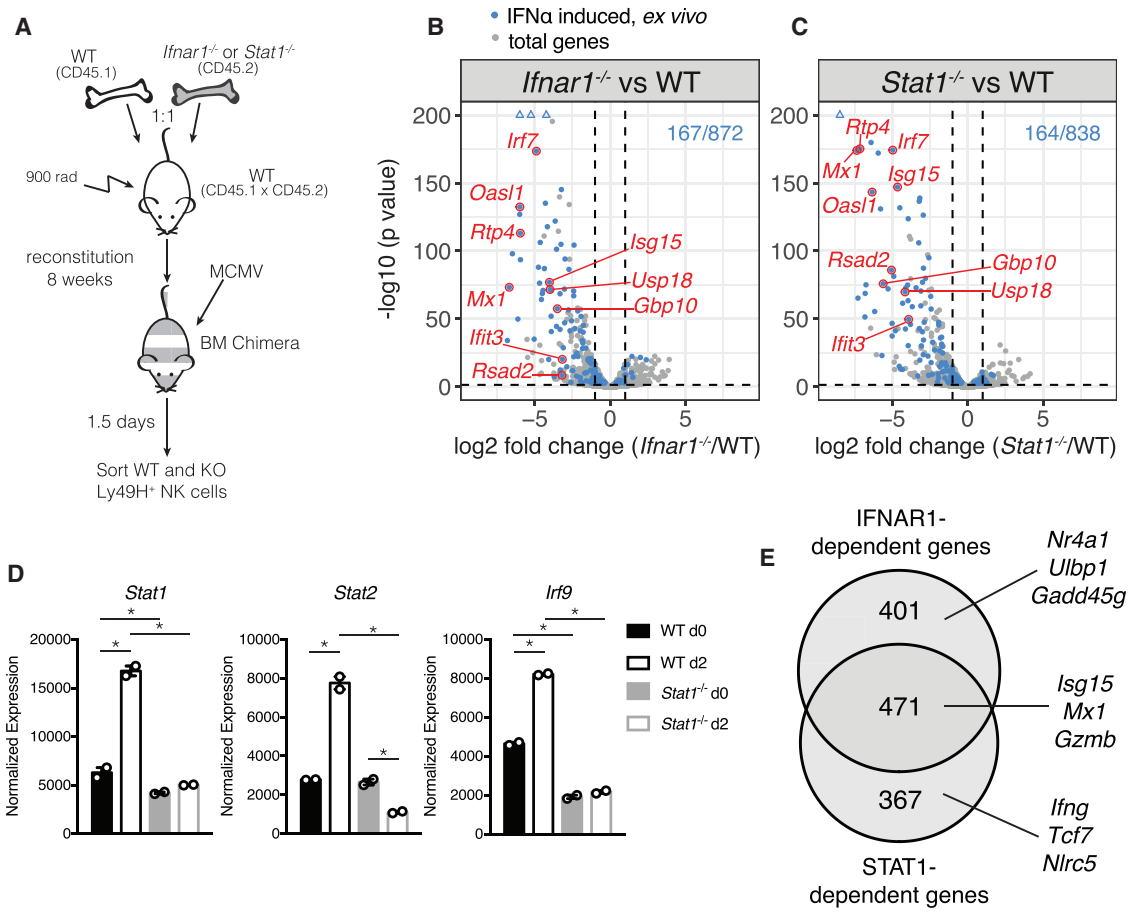

Figure 2. During MCMV Infection, a Subset of IFNAR1-Dependent Transcriptional Changes in NK Cells Are STAT1 Independent

(A) Schematic of experimental design. Briefly, mBMC mice harboring both WT and *Ifnar1*$^{-/-}$ or WT and *Stat1*$^{-/-}$ NK cells were infected with MCMV. Splenic Ly49H^{+} NK cells of each genotype were sorted for RNA-seq at 0 and 1.5 days PI (n = 1–3 per genotype per time point).

(B) Volcano plot of RNA-seq data comparing *Ifnar1*$^{-/-}$ and WT NK cells at day 1.5 PI. IFNα-inducible genes (i.e., differentially expressed genes in Figure 1) that are also differentially expressed in *Ifnar1*$^{-/-}$ versus WT NK cells are shown in blue, with select genes highlighted. Number of blue genes of total differentially expressed between *Ifnar1*$^{-/-}$ and WT NK cells at day 1.5 PI genes indicated at upper right.

(C) As in (B) but showing *Stat1*$^{-/-}$ versus WT.

(D) Normalized counts of *Stat1*, *Stat2*, and *Irf9* in WT and *Stat1*$^{-/-}$ NK cells from RNA-seq. Symbols represent biological replicates, and error bars show SEM (*p < 0.05).

(E) Overlap of differentially expressed genes between WT and *Ifnar1*$^{-/-}$ versus WT and *Stat1*$^{-/-}$ NK cells at day 1.5 PI.

contribute to the increased susceptibility of *Irf9*$^{-/-}$ mice to MCMV infection. However, because *Irf9*$^{-/-}$ NK cells can still produce IFN-γ, this may afford the *Irf9*$^{-/-}$ mice some degree of protection.

IRF9 Promotes Survival but not Proliferation of NK Cells following Viral Infection

To determine how IRF9 deficiency impaired NK cell expansion, we performed comparative transcriptome analysis by RNA-seq on purified WT and *Irf9*$^{-/-}$ Ly49H^{+} NK cells from mBMC 4 days post-MCMV infection, a time point immediately after *Irf9* expression peaks in WT cells (Figure 2D). The absence of IRF9 altered the expression of 1,008 genes (Figure 4A). Although similar numbers of genes were induced and repressed by IRF9, the most significant changes occurred in genes found to be downregulated in *Irf9*$^{-/-}$ cells relative to WT cells, and many of these were canonical ISGs (Figure 4A). Pathway analysis showed dysregulation of IFN signaling pathways (Figure S4A) but also revealed alterations in apoptosis signaling and lymphocyte activation pathways (Figure 4B). Labeling NK cells with the division-tracking dye CTV prior to adoptive transfer confirmed that IRF9 was dispensable for MCMV-driven NK cell proliferation (Figure 4C). In contrast, FLICA staining (to detect activated caspases) showed evidence of greater apoptosis in *Irf9*$^{-/-}$ NK cells (Figure 4D). Together, these findings suggest that IRF9 is required for NK cell survival, but not proliferation, following MCMV infection.

Previous studies have shown that IFNAR1-deficient lymphocytes are susceptible to killing by activated NK cells after viral infection because of lower expression of MHC I and higher expression of ligands for NK cell activating receptors (Crouse et al., 2014; Madera et al., 2016; Xu et al., 2014). Consistent

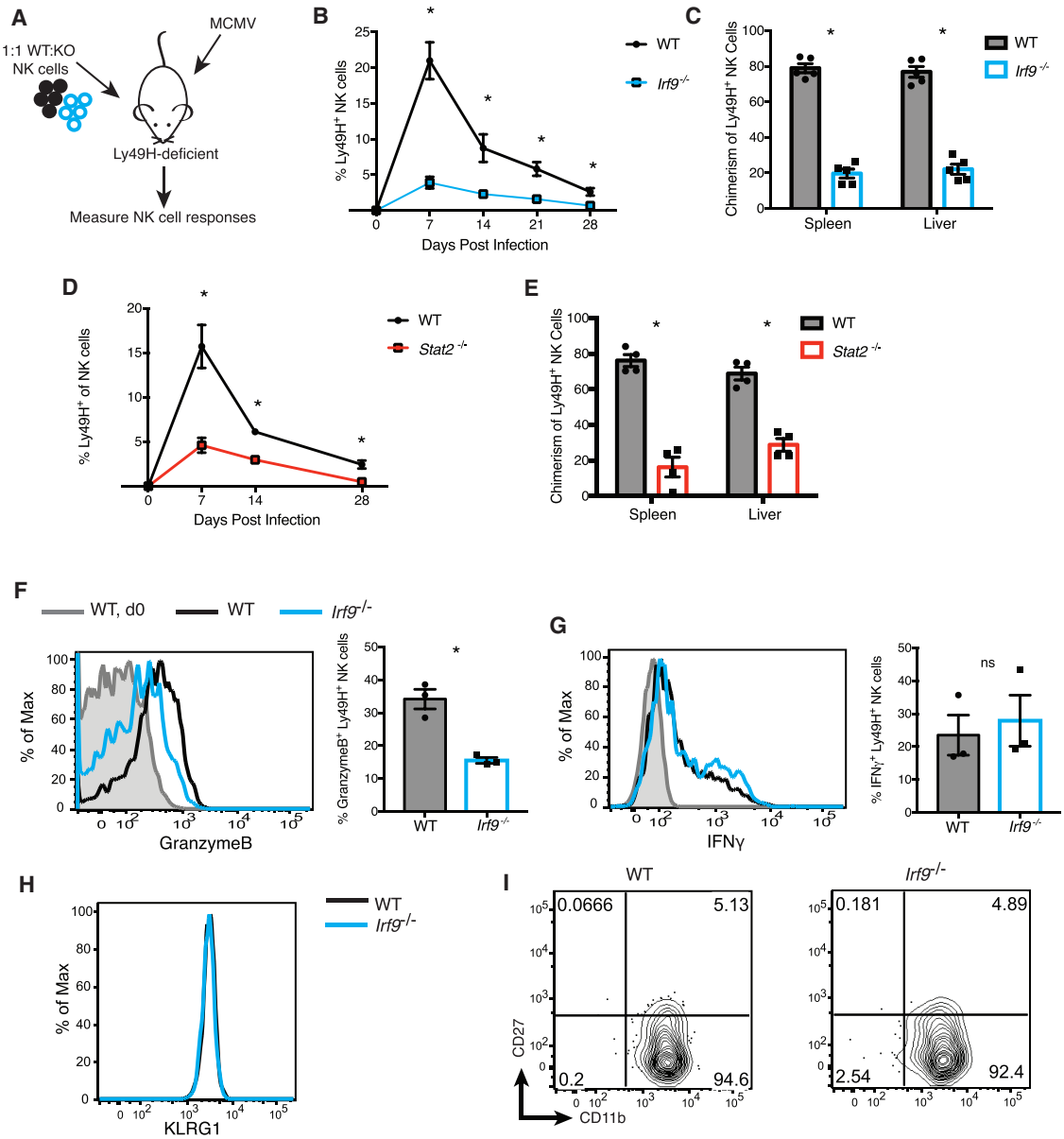

Figure 3. Non-redundant and Cell-Intrinsic Requirement for ISGF3 Components for the Optimal Expansion of Antiviral NK Cells

(A) Experimental schematic. Equal numbers of splenic Ly49H$^+$ KLRG1^{lo} NK cells from WT (CD45.1) and *Irf9*$^{-/-}$ or *Stat2*$^{-/-}$ mice (CD45.2) were co-transferred into Ly49H-deficient recipients prior to infection with MCMV.

(B) Absolute percentages of adoptively transferred WT versus *Irf9*$^{-/-}$ Ly49H$^+$ NK cells measured in peripheral blood at the indicated times following MCMV infection or inferred from transfer (day 0).

(C) Relative percentage of transferred WT and *Irf9*$^{-/-}$ Ly49H$^+$ NK cells in indicated organs at day 28 PI.

(D) As in (B), except that NK cells were transferred from WT and *Stat2*$^{-/-}$ mice.

(E) As in (C), except that NK cells were transferred from WT and *Stat2*$^{-/-}$ mice.

(F) Expression of intracellular granzyme B in splenic WT and Irf9$^{-/-}$ Ly49H$^+$ NK cells from mBMC animals on day 2 PI with MCMV.

(G) As in (F), except showing IFN-γ.

(H and I) KLRG1 (H) and CD27 and CD11b (I) expression were assessed in the blood 7 days PI with MCMV following co-adoptive transfer of WT and *Irf9*$^{-/-}$ cells, as in (B).

Data are representative of two (D–G) or three (B, C, H, and I) independent experiments with n = 3–5 mice per group. Symbols represent mean (B and D) or individual mice (C and E–G), and error bars show SEM (*$p < 0.05$).

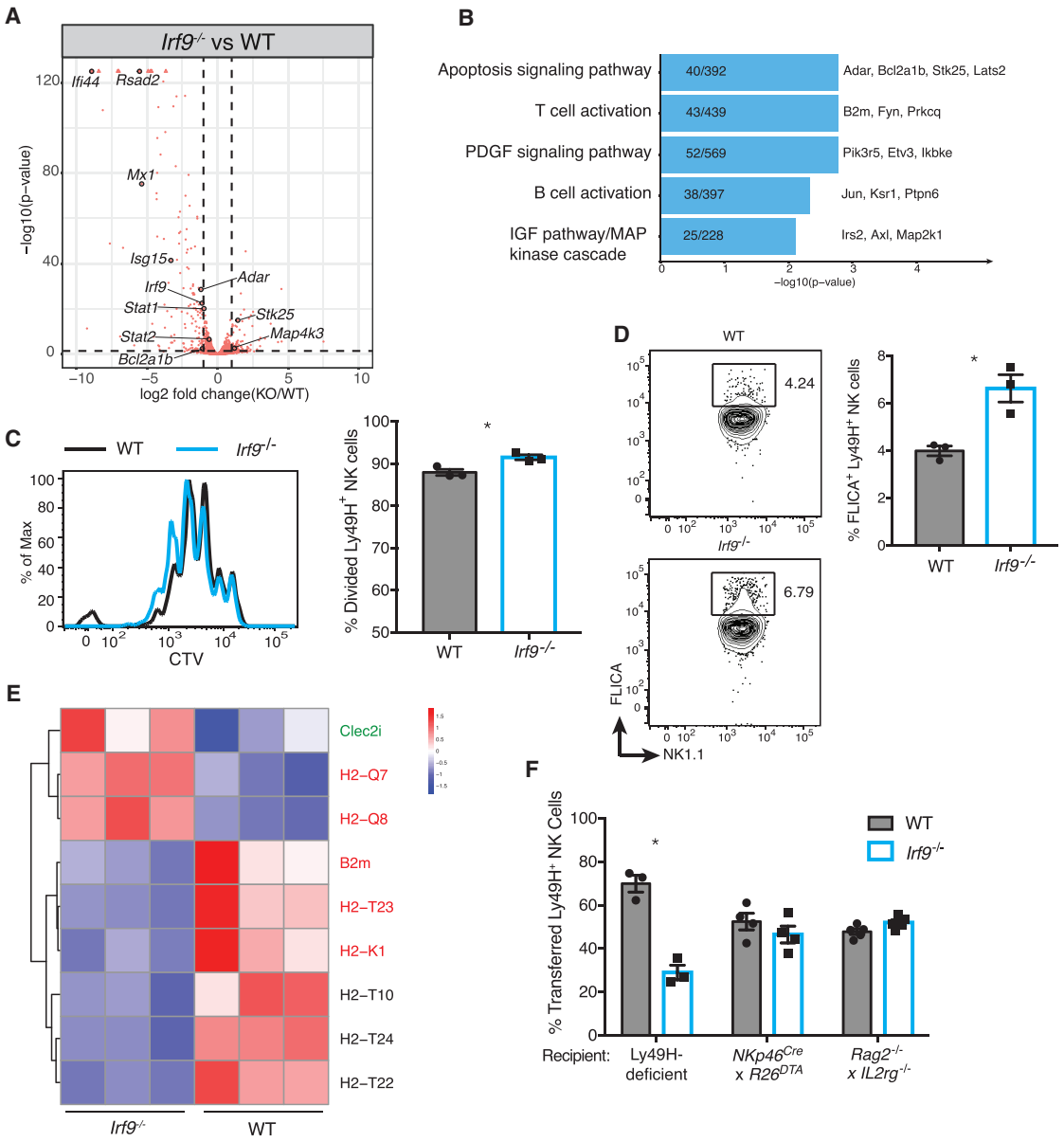

Figure 4. IRF9 Is Required for Survival but Not Proliferation of NK Cells following Viral Infection

mBMC mice harboring both WT and *Irf9*$^{-/-}$ NK cells were infected with MCMV. Splenic Ly49H^{+} WT and *Irf9*$^{-/-}$ NK cells were sorted for RNA-seq at 4 days PI (n = 3 per genotype).

(A) Volcano plot of RNA-seq data showing differentially expressed genes with genes of interest labeled. Horizontal line indicates p = 0.05, and vertical lines show absolute $\log_2$ fold change = 1.

(B) Top five enriched pathways as calculated using the PANTHER database, including number of differentially expressed genes per pathway and names of representative genes. Bar plots depict $-\log_{10}$ p values calculated using goseq.

(C) As in Figure 3A, except NK cells were labeled with CTV prior to adoptive co-transfer. Left: representative histogram of CTV in splenic WT and *Irf9*$^{-/-}$ Ly49H^{+} NK cells at day 3 PI. Right: quantification of Ly49H^{+} NK cells that divided more than once.

(D) Pan-caspase activation in transferred Ly49H^{+} NK cell populations in the spleen at day 4 PI.

(E) Heatmap of row-normalized $\log_2$-transformed counts of differentially expressed genes with putative roles in NK cell activation or inhibition. Experimentally validated activating ligands are green and experimentally validated inhibitory ligands are red.

(F) WT and *Irf9*$^{-/-}$ NK cells were co-transferred into Ly49H-deficient recipients as in Figure 3A or transferred into *Rag2*$^{-/-}$*Il2rg*$^{-/-}$ mice or *NKp46*^{Cre} *R26*^{DTA} mice. Data are representative of three independent experiments with n = 2–5 mice per group. Symbols represent individual mice, and error bars show SEM (*p < 0.05).

with these findings, our RNA-seq analysis revealed that *Irf9*$^{-/-}$ NK cells also have dysregulated expression of known and putative ligands for activating and inhibitory NK cell receptors following MCMV infection (Figure 4E), which may contribute to overall susceptibility to cytotoxicity. Specifically, *Irf9*$^{-/-}$ NK cells showed higher expression of *Clec2i,* which encodes Clr-g, a ligand for the activating receptor NKRP1f (Iizuka et al., 2003), and lower expression of several MHC class I molecules, including *H2-t23*, encoding the MHC class Ib molecule Qa-1b, which is critical for protecting activated T cells from lysis by NKG2A^{+} NK cells (Lu et al., 2007). Furthermore, of the molecules affected by IRF9 ablation, ChIP-seq showed that four of the nine genes had IRF9 binding to their promoters in NK cells stimulated with IFN-α (Figure S4B), suggesting direct IRF9-mediated regulation of these loci.

Previous work demonstrated that depletion of NK cells or transfer into NK cell-deficient hosts was sufficient to rescue the expansion defect of *Ifnar1*$^{-/-}$ T and NK cells (Crouse et al., 2014; Madera et al., 2016; Xu et al., 2014). Likewise, we found that following transfer into lymphocyte-deficient *Rag2*$^{-/-}$*IL2rg*$^{-/-}$ mice or NK cell-deficient (*NKp46*^{Cre} *R26*^{DTA}) mice, *Irf9*$^{-/-}$ cells expanded comparably with WT NK cells following MCMV infection (Figure 4F). Although the co-transferred WT NK cells in this setting are likely capable of fratricide, we hypothesized that they are not present in sufficient numbers to mediate appreciable levels of killing. Furthermore, *Irf9*$^{-/-}$ NK cells showed higher levels of cell death relative to WT NK cells when co-incubated with high ratios of activated effector NK cells (Figure S4C). Thus, IRF9-dependent sensing of type I IFNs during viral infection is necessary to protect activated NK cells against elimination by neighboring (host) NK cells.

In summary, we identified the total set of genes induced by IFN-α stimulation of purified NK cells and found that a subset of these genes, including *Stat1*, *Stat2*, and *Irf9*, were also induced during MCMV infection in a manner dependent on type I IFN signaling, suggesting an auto-regulatory loop in NK cells to support robust IFN-dependent antiviral responses. We used IRF9- and STAT2-deficient mice to demonstrate a non-redundant requirement for all three ISGF3 components in NK cell expansion and memory cell formation after MCMV. NK cells deficient in the type I IFN pathway proliferate normally but have dysregulated cell death pathways and altered expression of NK cell receptor ligands, making them susceptible to NK cell-mediated fratricide.

It is well established that NK cell cytotoxicity is triggered by weighing the balance of activating and inhibitory inputs (Joncker et al., 2009). Although NK cells have been shown to tolerate a wide range of MHC class I levels (Brodin et al., 2010; Jonsson et al., 2010), their tolerance of low levels of MHCI is significantly reduced in inflammatory settings (Ludigs et al., 2015; Sun and Lanier, 2008). Thus, it may not be surprising that subtle shifts in expression of a handful of cell surface molecules (activating and inhibitory ligands) would be causative of larger defects in the ability of ISGF3 component-deficient NK cells to expand following MCMV infection. We speculate that it is the combined impact of increased activating ligand and reduced MHC class I expression on proliferating *Irf9*$^{-/-}$ NK cells together with the heightened cytotoxic function of neighboring (WT host) NK cells that leads to fratricide during the antiviral response.

Previous studies have shown that expression of ISGF3 components increases following treatment of cells with IFNs or other cytokines and that this heightened expression can augment the induction of downstream ISGs (Ivashkiv and Donlin, 2014). However, this evidence has primarily been demonstrated in cell lines or macrophages stimulated with IFN-γ; here, we demonstrate that type I IFN signaling in primary lymphocytes is both necessary and sufficient to induce *Stat1*, *Stat2*, and *Irf9* expression *in vitro* and *in vivo* through an auto-regulatory mechanism. Such transcriptional auto-regulatory loops have been described across a range of systems and are important controllers of diverse processes ranging from bacterial pathogenicity (Zhang et al., 2013) to neuronal development (Bai et al., 2007) and cell cycle progression in eukaryotes (Johnson et al., 1994). That ISGF3 components in the mammalian immune system are also regulated in this manner likely allows lymphocytes to respond rapidly at the first sign of infection and highlights the importance of the type I IFN pathway in the host immune response.

Although our transcriptomic data were suggestive that non-canonical type I IFN signaling complexes might be activated in NK cells during viral infection (Figure 2E), adoptive transfer experiments with NK cells deficient in any member of the ISGF3 complex, or the upstream receptor, had a similar phenotype (i.e., an expansion defect due to fratricide). Thus, our data neither prove nor disprove the existence of non-canonical type I IFN signaling but demonstrate a critical, non-redundant function of individual ISGF3 components in antiviral NK cell defense. Furthermore, our study suggests that the dominant roles of the type I IFN pathway in NK cells during viral infection are to promote cytotoxicity (via upregulation of granzyme B) and protect against fratricide by proper regulation of cell surface receptors and ligands. Additionally, it is likely that other ISGs will have important functions in NK cells that are being masked by the overwhelming fratricide phenotype, and future studies are needed to address the potential roles of the ISGs identified in our *ex vivo* or *in vivo* experiments. A greater understanding of the molecular mechanisms underlying IFN signaling in activated lymphocytes will aid in our fight against a plethora of infectious diseases.

STAR★METHODS

Detailed methods are provided in the online version of this paper and include the following:

- KEY RESOURCES TABLE
- CONTACT FOR REAGENT AND RESOURCE SHARING
- EXPERIMENTAL MODEL AND SUBJECT DETAILS
  - Mice
  - Virus
  - Cell Lines
- METHOD DETAILS
  - Mixed Bone Marrow Chimeras
  - *In vivo* Virus Infection
  - Determination of Viral Titers

SUPPLEMENTAL INFORMATION

Supplemental Information includes four figures and can be found with this article online at https://doi.org/10.1016/j.celrep.2018.07.060.

ACKNOWLEDGMENTS

We thank members of the Sun and Leslie labs for technical support, experimental assistance, insightful comments, and helpful discussions. N.M.A. and S.V.G. were supported by a Medical Scientist Training Program grant from the NIH National Institute of General Medical Sciences (T32GM007739 to the Weill Cornell/Rockefeller/Sloan Kettering Tri-Institutional MD-PhD Program). N.M.A. was also supported by an F30 Predoctoral Fellowship from the NIH National Institute of Allergy and Infectious Diseases (F30 AI136239). C.M.L. was supported by a T32 award from the NIH (CA009149). A.R.T. was supported by the Novo Nordisk Foundation. C.S.L. was supported by NIH grant U01 HG007893. J.C.S. was supported by the Ludwig Center for Cancer Immunotherapy, the American Cancer Society, the Burroughs Wellcome Fund, and the NIH (AI100874, AI130043, and P30CA008748).

AUTHOR CONTRIBUTIONS

C.D.G., N.M.A., and S.V.G. performed experiments. C.D.G., C.K., C.M.L., Y.P., and C.S.L. analyzed the data. A.R.T. provided mice. C.D.G. and J.C.S. designed the study and wrote the manuscript.

DECLARATION OF INTERESTS

The authors declare no competing financial interests.

Received: February 16, 2018
Revised: June 5, 2018
Accepted: July 17, 2018
Published: August 21, 2018

REFERENCES

Arase, H., Mocarski, E.S., Campbell, A.E., Hill, A.B., and Lanier, L.L. (2002). Direct recognition of cytomegalovirus by activating and inhibitory NK cell receptors. Science *296*, 1323–1326.

Bai, G., Sheng, N., Xie, Z., Bian, W., Yokota, Y., Benezra, R., Kageyama, R., Guillemot, F., and Jing, N. (2007). Id sustains Hes1 expression to inhibit precocious neurogenesis by releasing negative autoregulation of Hes1. Dev. Cell *13*, 283–297.

Beaulieu, A.M., Zawislak, C.L., Nakayama, T., and Sun, J.C. (2014). The transcription factor Zbtb32 controls the proliferative burst of virus-specific natural killer cells responding to infection. Nat. Immunol. *15*, 546–553.

Bluyssen, H.A., and Levy, D.E. (1997). Stat2 is a transcriptional activator that requires sequence-specific contacts provided by stat1 and p48 for stable interaction with DNA. J. Biol. Chem. *272*, 4600–4605.

Bolger, A.M., Lohse, M., and Usadel, B. (2014). Trimmomatic: a flexible trimmer for Illumina sequence data. Bioinformatics *30*, 2114–2120.

Brodin, P., Lakshmikanth, T., Mehr, R., Johansson, M.H., Duru, A.D., Achour, A., Salmon-Divon, M., Kärre, K., Höglund, P., and Johansson, S. (2010). Natural killer cell tolerance persists despite significant reduction of self MHC class I on normal target cells in mice. PLoS ONE *5*, 5.

Brown, M.G., Dokun, A.O., Heusel, J.W., Smith, H.R., Beckman, D.L., Blattenberger, E.A., Dubbelde, C.E., Stone, L.R., Scalzo, A.A., and Yokoyama, W.M. (2001). Vital involvement of a natural killer cell activation receptor in resistance to viral infection. Science *292*, 934–937.

Crouse, J., Bedenikovic, G., Wiesel, M., Ibberson, M., Xenarios, I., Von Laer, D., Kalinke, U., Vivier, E., Jonjic, S., and Oxenius, A. (2014). Type I interferons protect T cells against NK cell attack mediated by the activating receptor NCR1. Immunity *40*, 961–973.

Daniels, K.A., Devora, G., Lai, W.C., O'Donnell, C.L., Bennett, M., and Welsh, R.M. (2001). Murine cytomegalovirus is regulated by a discrete subset of natural killer cells reactive with monoclonal antibody to Ly49H. J. Exp. Med. *194*, 29–44.

Dokun, A.O., Kim, S., Smith, H.R., Kang, H.S., Chu, D.T., and Yokoyama, W.M. (2001). Specific and nonspecific NK cell activation during virus infection. Nat. Immunol. *2*, 951–956.

Fink, K., and Grandvaux, N. (2013). STAT2 and IRF9: beyond ISGF3. JAK-STAT *2*, e27521.

Fodil-Cornu, N., Lee, S.H., Belanger, S., Makrigiannis, A.P., Biron, C.A., Buller, R.M., and Vidal, S.M. (2008). Ly49h-deficient C57BL/6 mice: a new mouse cytomegalovirus-susceptible model remains resistant to unrelated pathogens controlled by the NK gene complex. J. Immunol. *181*, 6394–6405.

Geary, C.D., and Sun, J.C. (2017). Memory responses of natural killer cells. Semin. Immunol. *31*, 11–19.

Gil, M.P., Bohn, E., O'Guin, A.K., Ramana, C.V., Levine, B., Stark, G.R., Virgin, H.W., and Schreiber, R.D. (2001). Biologic consequences of Stat1-independent IFN signaling. Proc. Natl. Acad. Sci. USA *98*, 6680–6685.

Guan, J., Miah, S.M., Wilson, Z.S., Erick, T.K., Banh, C., and Brossay, L. (2014). Role of type I interferon receptor signaling on NK cell development and functions. PLoS ONE *9*, e111302.

Hahne, F., and Ivanek, R. (2016). Visualizing genomic data using Gviz and Bioconductor. Methods Mol. Biol. *1418*, 335–351.

Hofer, M.J., Li, W., Manders, P., Terry, R., Lim, S.L., King, N.J., and Campbell, I.L. (2012). Mice deficient in STAT1 but not STAT2 or IRF9 develop a lethal CD4+ T-cell-mediated disease following infection with lymphocytic choriomeningitis virus. J. Virol. *86*, 6932–6946.

Iizuka, K., Naidenko, O.V., Plougastel, B.F., Fremont, D.H., and Yokoyama, W.M. (2003). Genetically linked C-type lectin-related ligands for the NKRP1 family of natural killer cell receptors. Nat. Immunol. *4*, 801–807.

Ivashkiv, L.B., and Donlin, L.T. (2014). Regulation of type I interferon responses. Nat. Rev. Immunol. *14*, 36–49.

Johnson, D.G., Ohtani, K., and Nevins, J.R. (1994). Autoregulatory control of E2F1 expression in response to positive and negative regulators of cell cycle progression. Genes Dev. *8*, 1514–1525.

Johnson, L.R., Weizman, O.E., Rapp, M., Way, S.S., and Sun, J.C. (2016). Epitope-specific vaccination limits clonal expansion of heterologous naive T cells during viral challenge. Cell Rep *17*, 636–644.

Joncker, N.T., Fernandez, N.C., Treiner, E., Vivier, E., and Raulet, D.H. (2009). NK cell responsiveness is tuned commensurate with the number of inhibitory receptors for self-MHC class I: the rheostat model. J. Immunol. *182*, 4572–4580.

Jonsson, A.H., Yang, L., Kim, S., Taffner, S.M., and Yokoyama, W.M. (2010). Effects of MHC class I alleles on licensing of Ly49A+ NK cells. J. Immunol. *184*, 3424–3432.

Kamimura, Y., and Lanier, L.L. (2014). Rapid and sequential quantitation of salivary gland-associated mouse cytomegalovirus in oral lavage. J. Virol. Methods *205*, 53–56.

Kent, W.J., Zweig, A.S., Barber, G., Hinrichs, A.S., and Karolchik, D. (2010). BigWig and BigBed: enabling browsing of large distributed datasets. Bioinformatics *26*, 2204–2207.

Kimura, T., Kadokawa, Y., Harada, H., Matsumoto, M., Sato, M., Kashiwazaki, Y., Tarutani, M., Tan, R.S., Takasugi, T., Matsuyama, T., et al. (1996). Essential and non-redundant roles of p48 (ISGF3 gamma) and IRF-1 in both type I and type II interferon responses, as revealed by gene targeting studies. Genes Cells *1*, 115–124.

Langmead, B., and Salzberg, S.L. (2012). Fast gapped-read alignment with Bowtie 2. Nat. Methods *9*, 357–359.

Lanier, L.L. (2008). Up on the tightrope: natural killer cell activation and inhibition. Nat. Immunol. *9*, 495–502.

Lawrence, M., Huber, W., Pagès, H., Aboyoun, P., Carlson, M., Gentleman, R., Morgan, M.T., and Carey, V.J. (2013). Software for computing and annotating genomic ranges. PLoS Comput. Biol. *9*, e1003118.

Levy, D.E., Kessler, D.S., Pine, R., and Darnell, J.E., Jr. (1989). Cytoplasmic activation of ISGF3, the positive regulator of interferon-alpha-stimulated transcription, reconstituted in vitro. Genes Dev. *3*, 1362–1371.

Li, Q.H., Brown, J.B., Huang, H.Y., and Bickel, P.J. (2011). Measuring reproducibility of high-throughput experiments. Ann. Appl. Stat. *5*, 1752–1779.

Love, M.I., Huber, W., and Anders, S. (2014). Moderated estimation of fold change and dispersion for RNA-seq data with DESeq2. Genome Biol. *15*, 550.

Lu, L., Ikizawa, K., Hu, D., Werneck, M.B., Wucherpfennig, K.W., and Cantor, H. (2007). Regulation of activated CD4+ T cells by NK cells via the Qa-1-NKG2A inhibitory pathway. Immunity *26*, 593–604.

Ludigs, K., Seguín-Estévez, Q., Lemeille, S., Ferrero, I., Rota, G., Chelbi, S., Mattmann, C., MacDonald, H.R., Reith, W., and Guarda, G. (2015). NLRC5 exclusively transactivates MHC class I and related genes through a distinctive SXY module. PLoS Genet. *11*, e1005088.

Luker, K.E., Pica, C.M., Schreiber, R.D., and Piwnica-Worms, D. (2001). Overexpression of IRF9 confers resistance to antimicrotubule agents in breast cancer cells. Cancer Res. *61*, 6540–6547.

Madera, S., Rapp, M., Firth, M.A., Beilke, J.N., Lanier, L.L., and Sun, J.C. (2016). Type I IFN promotes NK cell expansion during viral infection by protecting NK cells against fratricide. J. Exp. Med. *213*, 225–233.

Madera, S., Geary, C.D., Lau, C.M., Pikovskaya, O., Reiner, S.L., and Sun, J.C. (2018). Cutting edge: divergent requirement of T-box transcription factors in effector and memory NK cells. J. Immunol. *200*, 1977–1981.

Majoros, A., Platanitis, E., Kernbauer-Hölzl, E., Rosebrock, F., Müller, M., and Decker, T. (2017). Canonical and non-canonical aspects of JAK-STAT signaling: lessons from interferons for cytokine responses. Front. Immunol. *8*, 29.

Meraz, M.A., White, J.M., Sheehan, K.C., Bach, E.A., Rodig, S.J., Dighe, A.S., Kaplan, D.H., Riley, J.K., Greenlund, A.C., Campbell, D., et al. (1996). Targeted disruption of the Stat1 gene in mice reveals unexpected physiologic specificity in the JAK-STAT signaling pathway. Cell *84*, 431–442.

Mizutani, T., Neugebauer, N., Putz, E.M., Moritz, N., Simma, O., Zebedin-Brandl, E., Gotthardt, D., Warsch, W., Eckelhart, E., Kantner, H.P., et al. (2012). Conditional IFNAR1 ablation reveals distinct requirements of Type I IFN signaling for NK cell maturation and tumor surveillance. OncoImmunology *1*, 1027–1037.

Müller, U., Steinhoff, U., Reis, L.F., Hemmi, S., Pavlovic, J., Zinkernagel, R.M., and Aguet, M. (1994). Functional role of type I and type II interferons in antiviral defense. Science *264*, 1918–1921.

Narni-Mancinelli, E., Chaix, J., Fenis, A., Kerdiles, Y.M., Yessaad, N., Reynders, A., Gregoire, C., Luche, H., Ugolini, S., Tomasello, E., et al. (2011). Fate mapping analysis of lymphoid cells expressing the NKp46 cell surface receptor. Proc. Natl. Acad. Sci. USA *108*, 18324–18329.

Park, C., Li, S., Cha, E., and Schindler, C. (2000). Immune response in Stat2 knockout mice. Immunity *13*, 795–804.

Perry, S.T., Buck, M.D., Lada, S.M., Schindler, C., and Shresta, S. (2011). STAT2 mediates innate immunity to Dengue virus in the absence of STAT1 via the type I interferon receptor. PLoS Pathog. *7*, e1001297.

Quinlan, A.R., and Hall, I.M. (2010). BEDTools: a flexible suite of utilities for comparing genomic features. Bioinformatics *26*, 841–842.

Qureshi, S.A., Salditt-Georgieff, M., and Darnell, J.E., Jr. (1995). Tyrosine-phosphorylated Stat1 and Stat2 plus a 48-kDa protein all contact DNA in forming interferon-stimulated-gene factor 3. Proc. Natl. Acad. Sci. USA *92*, 3829–3833.

Rapp, M., Lau, C.M., Adams, N.M., Weizman, O.E., O'Sullivan, T.E., Geary, C.D., and Sun, J.C. (2017). Core-binding factor β and Runx transcription factors promote adaptive natural killer cell responses. Sci. Immunol. *2*, 2.

Smith, H.R., Heusel, J.W., Mehta, I.K., Kim, S., Dorner, B.G., Naidenko, O.V., Iizuka, K., Furukawa, H., Beckman, D.L., Pingel, J.T., et al. (2002). Recognition of a virus-encoded ligand by a natural killer cell activation receptor. Proc. Natl. Acad. Sci. USA *99*, 8826–8831.

Speir, M.L., Zweig, A.S., Rosenbloom, K.R., Raney, B.J., Paten, B., Nejad, P., Lee, B.T., Learned, K., Karolchik, D., Hinrichs, A.S., et al. (2016). The UCSC Genome Browser database: 2016 update. Nucleic Acids Res. *44* (*D1*), D717–D725.

Sun, J.C., and Lanier, L.L. (2008). Cutting edge: viral infection breaks NK cell tolerance to "missing self". J. Immunol. *181*, 7453–7457.

Sun, J.C., and Lanier, L.L. (2011). NK cell development, homeostasis and function: parallels with $CD8^+$ T cells. Nat. Rev. Immunol. *11*, 645–657.

Sun, J.C., Beilke, J.N., and Lanier, L.L. (2009). Adaptive immune features of natural killer cells. Nature *457*, 557–561.

Sun, J.C., Madera, S., Bezman, N.A., Beilke, J.N., Kaplan, M.H., and Lanier, L.L. (2012). Proinflammatory cytokine signaling required for the generation of natural killer cell memory. J. Exp. Med. *209*, 947–954.

Veals, S.A., Santa Maria, T., and Levy, D.E. (1993). Two domains of ISGF3 gamma that mediate protein-DNA and protein-protein interactions during transcription factor assembly contribute to DNA-binding specificity. Mol. Cell. Biol. *13*, 196–206.

Viant, C., Guia, S., Hennessy, R.J., Rautela, J., Pham, K., Bernat, C., Goh, W., Jiao, Y., Delconte, R., Roger, M., et al. (2017). Cell cycle progression dictates the requirement for BCL2 in natural killer cell survival. J. Exp. Med. *214*, 491–510.

Voigt, V., Forbes, C.A., Tonkin, J.N., Degli-Esposti, M.A., Smith, H.R., Yokoyama, W.M., and Scalzo, A.A. (2003). Murine cytomegalovirus m157 mutation and variation leads to immune evasion of natural killer cells. Proc. Natl. Acad. Sci. USA *100*, 13483–13488.

Wesoly, J., Szweykowska-Kulinska, Z., and Bluyssen, H.A. (2007). STAT activation and differential complex formation dictate selectivity of interferon responses. Acta Biochim. Pol. *54*, 27–38.

Xu, H.C., Grusdat, M., Pandyra, A.A., Polz, R., Huang, J., Sharma, P., Deenen, R., Köhrer, K., Rahbar, R., Diefenbach, A., et al. (2014). Type I interferon protects antiviral CD8+ T cells from NK cell cytotoxicity. Immunity *40*, 949–960.

Young, M.D., Wakefield, M.J., Smyth, G.K., and Oshlack, A. (2010). Gene ontology analysis for RNA-seq: accounting for selection bias. Genome Biol. *11*, R14.

Zhang, Y., Liu, T., Meyer, C.A., Eeckhoute, J., Johnson, D.S., Bernstein, B.E., Nusbaum, C., Myers, R.M., Brown, M., Li, W., and Liu, X.S. (2008). Model-based analysis of ChIP-Seq (MACS). Genome Biol. *9*, R137.

Zhang, Y., Wang, L., Han, Y., Yan, Y., Tan, Y., Zhou, L., Cui, Y., Du, Z., Wang, X., Bi, Y., et al. (2013). Autoregulation of PhoP/PhoQ and positive regulation of the cyclic AMP receptor protein-cyclic AMP complex by PhoP in Yersinia pestis. J. Bacteriol. *195*, 1022–1030.

Zheng, Y., Josefowicz, S.Z., Kas, A., Chu, T.T., Gavin, M.A., and Rudensky, A.Y. (2007). Genome-wide analysis of Foxp3 target genes in developing and mature regulatory T cells. Nature *445*, 936–940.

Zhu, L.J., Gazin, C., Lawson, N.D., Pagès, H., Lin, S.M., Lapointe, D.S., and Green, M.R. (2010). ChIPpeakAnno: a Bioconductor package to annotate ChIP-seq and ChIP-chip data. BMC Bioinformatics *11*, 237.

STAR★METHODS

KEY RESOURCES TABLE

REAGENT or RESOURCE	SOURCE	IDENTIFIER
Antibodies		
Anti-Mouse CD3ε (clone 17A2)	Tonbo Biosciences	Cat#25-0032; RRID:AB_2621619
Anti-Mouse TCRβ (clone H57-597)	BioLegend	Cat#109220; RRID:AB_893624
Anti-Mouse CD19 (clone 6D5)	BioLegend	Cat#115530; RRID:AB_830707
Anti-Mouse F4/80 (clone BM8.1)	BioLegend	Cat#123117; RRID:AB_893489
Anti-Mouse NK1.1 (clone PK136)	Tonbo Biosciences	Cat#65-5941; RRID:AB_2621910
Anti-Mouse NKp46 (clone 29A1.4)	BioLegend	Cat#137604; RRID:AB_2235755
Anti-Mouse Ly49H (clone 3D10)	eBioscience	Cat#11-5886-81; RRID:AB_1257160
Anti-Mouse CD45.1 (clone A20)	BioLegend	Cat#110729; RRID:AB_1134170
Anti-Mouse CD45.2 (clone 104)	BioLegend	Cat#109821; RRID:AB_493730
Anti-Mouse CD49b (clone Dx5)	BioLegend	Cat#108918; RRID: AB_2265144
Annexin V	BioLegend	Cat# 640943, RRID:AB_2616658
Anti-Mouse/Human CD11b (clone M1/70)	BioLegend	Cat#101223; RRID:AB_755985
Anti-CD27 (clone LG.7F9)	eBioscience	Cat#14-0271-81; RRID:AB_467182
Anti-Mouse KLRG1 (clone 2F1)	Tonbo Biosciences	Cat#50-5893; RRID:AB_2621800
Anti-Mouse Ly49D (clone 4E5)	BioLegend	Cat#138308; RRID:AB_10639939
Anti-Mouse Ly49A (clone YE1/48.10.6)	BioLegend	Cat#116810; RRID:AB_572013
Anti-Mouse Ly49C and Ly49I (clone 5E6)	BD Biosciences	Cat#553277; RRID:AB_394751
Anti-Mouse CD69 (clone H1.2F3)	BioLegend	Cat#104524; RRID:AB_2074979
Anti-Human/Mouse Granzyme B (clone GB11)	BioLegend	Cat#515403; RRID:AB_2114575
Anti-Mouse IFN gamma (clone XMG1.2)	Tonbo Biosciences	Cat#20-7311; RRID:AB_2621616
Anti-Mouse CD107a (clone 1D4B)	BioLegend	Cat#121611; RRID:AB_1732051
Anti-NK1.1 depletion antibody (clone PK136	J. Sun (PI)	N/A
InVivoMab Anti-Mouse CD8α (NK cell enrichment, clone 2.43)	Bio X Cell	Cat#BE0061; RRID:AB_1125541
InVivoMab Anti-Mouse CD4 (NK cell enrichment, clone GK1.5)	Bio X Cell	Cat#BE0003-1; RRID:AB_1107636
InVivoMab Anti-Mouse CD19 (NK cell enrichment, clone 1D3)	Bio X Cell	Cat#BE0150; RRID:AB_10949187
InVivoMab Anti-Mouse Ter-119 (NK cell enrichment, clone TER-119)	Bio X Cell	Cat#BE0183; RRID:AB_10949625
Anti-IRF9: ISGF-3gamma p48 (C-20) (ChIP, polyclonal)	Santa Cruz Biotechnology	Cat#sc-496; RRID:AB_2127709
Anti-STAT1 (M-22) (ChIP, polyclonal)	Santa Cruz Biotechnology	Cat#sc-592; RRID:AB_632434
Bacterial and Virus Strains		
Murine Cytomegalovirus (MCMV)	J. Sun (PI)	Smith Strain
Chemicals, Peptides, and Recombinant Proteins		
Recombinant Mouse IL-12 Protein	R&D Sytems	Cat#419-ML
Recombinant Mouse IL-18	MBL	Cat#B002-5
Recombinant Mouse IL-2 Protein	R&D Systems	Cat#402-ML
Recombinant Mouse IFNa 1 Protein	R&D Systems	Cat#12105-1
Phorbol 12-myristate 13-acetate (PMA)	Sigma-Aldrich	Cat#P8139
Ionomycin calcium salt from *Streptomyces conglobatus* (Ionomycin)	Sigma-Aldrich	Cat#I0634

(*Continued on next page*)

Continued

REAGENT or RESOURCE	SOURCE	IDENTIFIER
Critical Commercial Assays		
QIAamp DNA Blood Mini Kit	QIAGEN	Cat#51106
TRIzol Reagent	Thermo Fisher Scientific	Cat#15596026
Foxp3 Transcription Factor Staining Buffer Set	Thermo Fisher Scientific	Cat#00-5523-00
iQ SYBR Green Supermix	Bio-Rad	Cat#1708880
BioMag Goat Anti-Rat IgG (NK cell enrichment)	QIAGEN	Cat#310107
CellTrace Violet Cell Proliferation Kit	Thermo Fisher Scientific	Cat#C34557
Fixable Viability Dye eFluor 506	eBioscience	Cat#65-0866-18
FAM FLICA Poly Caspase Kit	Bio-Rad	Cat#ICT092
Deposited Data		
Raw Data Files for RNA and ChIP Sequencing	NCBI Gene Expression Omnibus	GSE106139
Experimental Models: Cell Lines		
Ba/F3	L. Lanier (PI)	N/A
Ba/F3-m157	L. Lanier (PI) (Voigt et al., 2003)	N/A
Experimental Models: Organisms/Strains		
Mouse: WT or CD45.2: C57BL/6J	The Jackson Laboratory	Stock#000644; RRID:IMSR_JAX:000664
Mouse: WT or CD45.1: B6.SJL-*Ptprc*^{a} *Pepc*^{b}/BoyJ	The Jackson Laboratory	Stock#002014; RRID:IMSR_JAX:002014
Mouse: CD45.1xCD45.2	J. Sun (PI)	N/A
Mouse: *Irf9*$^{-/-}$	A. Thomsen (PI) (Kimura et al., 1996)	N/A
Mouse: R26^{DTA}: *B6.129P2-Gt(ROSA)26Sor*$^{tm1(DTA)Lky}$/J	The Jackson Laboratory	Stock#009669; RRID: IMSR_JAX:009669
Mouse: *Nkp46*^{iCre}	E. Vivier (PI) (Narni-Mancinelli et al., 2011)	N/A
Mouse: Nkp46^{Cre} R26^{DTA}	J. Sun (PI)	N/A
Mouse: Ifnar1$^{-/-}$: B6(Cg)-Ifnar1$^{tm1.2Ees}$/J	The Jackson Laboratory	Stock#028288; RRID: IMSR_JAX:028288
Mouse: Stat1$^{-/-}$	R. Schreiber (PI) (Meraz et al., 1996)	N/A
Mouse: *Rag2*$^{-/-}$ *IL2rg*$^{-/-}$: C;129S4-*Rag2*$^{tm1.1Flv}$ *Il2rg*$^{tm1.1Flv}$/J	The Jackson Laboratory	Stock#014593; RRID:IMSR_JAX:014593
Mouse: *Klra8*$^{-/-}$ or Ly49H-deficient	S. Vidal (PI) (Fodil-Cornu et al., 2008)	N/A
Mouse: *Stat2*$^{-/-}$*: B6.129-Stat2*^{tm1Shnd}/J	The Jackson Laboratory	Stock#023309; RRID: IMSR_JAX:023309
Oligonucleotides		
Primers against MCMV IE-1 (F: TCGCCCATCGTTTCGAGA, R: TCTCGTAGGTCCACTGACGGA	Johnson et al., 2016	N/A
Software and Algorithms		
DESeq2 (v.1.14.1)	Love et al., 2014	http://bioconductor.org/packages/release/bioc/html/DESeq2.html
Trimmomatic (v.0.36)	Bolger et al., 2014	http://www.usadellab.org/cms/?page=trimmomatic
Bowtie2 (v2.2.9)	Langmead and Salzberg, 2012	http://bowtie-bio.sourceforge.net/bowtie2/index.shtml
GenomicAlignments (v.1.10.1)	Lawrence et al., 2013	https://bioconductor.org/packages/release/bioc/html/GenomicAlignments.html
bedtools2 (v2.26.0)	Quinlan and Hall, 2010	https://github.com/arq5x/bedtools2
bedGraphToBigWig (v.4)	Kent et al., 2010	http://hgdownload.soe.ucsc.edu/downloads.html#utilities_downloads

(*Continued on next page*)

Continued

REAGENT or RESOURCE	SOURCE	IDENTIFIER
Gviz (v.1.18.2)	Hahne and Ivanek, 2016	http://bioconductor.org/packages/release/bioc/html/Gviz.html
R (v.3.3.2)	https://www.r-project.org/	https://www.r-project.org/
MACS2 (v2.1.1.20160309)	Zhang et al., 2008	https://github.com/taoliu/MACS
ChipPeakAnno	Zhu et al., 2010	https://bioconductor.org/packages/release/bioc/html/ChIPpeakAnno.html
UCSC mm10 Known Gene Annotation Package	Speir et al., 2016	https://bioconductor.org/packages/release/data/annotation/html/TxDb.Mmusculus.UCSC.mm10.knownGene.html
Irreproducible Discovery Rate (IDR)	Li et al., 2011	https://www.encodeproject.org/software/idr/
goseq (v1.32.0)	Young et al., 2010	https://bioconductor.org/packages/release/bioc/html/goseq.html

CONTACT FOR REAGENT AND RESOURCE SHARING

Further information and requests for resources and reagents should be directed to and will be fulfilled by the Lead Contact, Joseph Sun (sunj@mskcc.org).

EXPERIMENTAL MODEL AND SUBJECT DETAILS

Mice

All mice used in this study were housed and bred under specific pathogen-free conditions at Memorial Sloan Kettering Cancer Center (MSKCC) in accordance with all guidelines of the Institutional Animal Care and Use Committee. This study used the following mouse strains, all on the C57BL/6 genetic background: C57BL/6 (CD45.2; The Jackson Laboratory), B6.SJL (CD45.1; Taconic), *Ifnar1*$^{-/-}$ (Müller et al., 1994), *Stat1*$^{-/-}$ (Meraz et al., 1996), *Stat2*$^{-/-}$ (Park et al., 2000) (JAX stock #023309), *Irf9*$^{-/-}$ (Kimura et al., 1996), *Klra8*$^{-/-}$ (Ly49H deficient; (Fodil-Cornu et al., 2008)), *Nkp46iCre* (referred to as *NKp46*^{Cre}; (Narni-Mancinelli et al., 2011)), *Rag2*$^{-/-}$ *Il2rg*$^{-/-}$ (Taconic), and *R26*^{DTA} (The Jackson Laboratory). *NKp46*^{Cre} *x R26*^{DTA} mice were generated at MSKCC. Experiments were conducted using age- and gender-matched mice in accordance with approved institutional protocols. Animals were typically 6-10 weeks old at the time of use and consisted of males and females.

Virus

MCMV (Smith strain) was serially passaged through BALB/c hosts twice, then viral stocks were prepared by dissociating salivary glands 3 weeks after infection with a dounce homogenizer.

Cell Lines

Ba/F3 cells were maintained at 37C in RPMI medium 1640 containing 10% FBS, 1mM sodium pyruvate, 2 mM glutamine, 1 mM HEPES, and 100 μg/mL penicillin/streptomycin. Ba/F3-m157 (Voigt et al., 2003) were maintained in the same conditions with the addition of 1 μM puromycin.

METHOD DETAILS

Mixed Bone Marrow Chimeras

Mixed bone marrow chimeric mice were generated by lethally irradiating (900 cGy) host CD45.1xCD45.2 mice, which were reconstituted with a 1:1 mixture of bone marrow cells from WT (CD45.1) and genetic-deficient (CD45.2) donor mice. Hosts were co-injected with anti-NK1.1 (clone PK136) to deplete any residual donor or host mature NK cells. Host CD45.1^{+} CD45.2^{+} NK cells were excluded from all analyses.

In vivo Virus Infection

Adoptive transfer studies were performed by mixing splenocytes from WT (CD45.1) and genetic-deficient (CD45.2) mice to achieve equal numbers of Ly49H^{+}KLRG1^{lo} NK cells, and injecting intravenously into adult Ly49H-deficient mice 1 day prior to MCMV infection. Recipient mice in adoptive transfer studies were infected by i.p. injection of 7.5 × 10^{2} PFU of MCMV. Experimental mixed bone marrow chimera mice were infected by i.p. injection of 7.5 × 10^{3} PFU of MCMV. For survival studies, mice were infected by i.p. injection of 4 × 10^{4} PFU of MCMV.

Determination of Viral Titers

Viral titers were determined as previously described (Kamimura and Lanier, 2014). DNA was isolated from peripheral blood using a genomic purification kit (QIAGEN). Following isolation, DNA concentration was measured using Nanodrop for each sample, and 3 μL was added into mastermix containing iQ Sybr Green (Bio-Rad) and primers specific to MCMV IE-1 DNA (forward: TCGCCCATCGTTTCGAGA, reverse: TCTCGTAGGTCCACTGACCGA). Copy number was determined by comparing Cq values to a standard curve of known dilutions of an MCMV plasmid and normalizing relative to total DNA content.

Isolation of Lymphocytes

Spleens were dissociated using glass slides and filtered through a 100-mm strainer. To isolate lymphocytes from liver, the tissue was physically dissociated using a glass tissue homogenizer and purified using a discontinuous gradient of 40% over 60% Percoll. To isolate cells from the lung, the tissue was physically dissociated using scissors and incubated for 30 min in digest solution (1 mg/mL type D collagenase in RPMI supplemented with 5% fetal calf serum, 1% L-glutamine, 1% penicillin-streptomycin, and 10 mM HEPES). Resulting dissociated tissue was passed through 100-mm strainers, centrifuged, and lymphocytes were removed from the supernatant. To isolate bone marrow lymphocytes, cleaned femur and tibia bones were ground with mortar and pestle, and the resulting solution filtered through a 100-mm strainer. To isolate the stromal vascular fraction (SVF) of adipose tissue, visceral adipose tissue was physically dissociated using scissors and incubated for 40 min in digest solution (2mg/ml type II collagenase in RPMI supplemented with 5% fetal calf serum, 1% L-glutamine, 1% penicillin-streptomycin, and 10 mM HEPES). Resulting dissociated tissue was passed through 100-mm strainers, centrifuged, and adipocytes were removed from the supernatant. Red blood cells in spleen, liver, lung, adipose and bone marrow were lysed using ACK lysis buffer.

Flow Cytometry and Cell Sorting

Cell surface staining of single-cell suspensions from various organs was performed using fluorophore-conjugated antibodies (BD Biosciences, eBioscience, BioLegend, Tonbo, R&D Systems). Intracellular staining was performed by fixing and permeabilizing with the eBioscience Foxp3/Transcription Factor Staining Set for staining intranuclear proteins and cytokines.

Flow cytometry and cell sorting were performed on the LSR II and Aria II cytometers (BD Biosciences), respectively. For RNA-Seq experiments, cell population were sorted to > 95% purity. Data were analyzed with FlowJo software (Tree Star). Flow cytometry of purified lymphocytes was performed using the following fluorophore-conjugated antibodies: CD3ε (17A2), TCRβ (H57-597), CD19 (ID3), F4/80 (BM8.1), NK1.1 (PK136), Ly49H (3D10), CD45.1 (A20), CD45.2 (104), CD11b (M1/70), CD27 (LG.3A10), KLRG1 (2F1), Ly49D (4E5), Ly49A (YE1/48.10.6), Ly49C/I (5E6), CD69 (H1.2F3), Granzyme B (GB11), IFN-γ (XMG1.2), CD107a (1D4B), and CD49b (DX5).

Apoptosis was evaluated by caspase activity staining using the carboxyfluorescein FLICA poly caspase assay kit (BioRad) or Annexin V (BioLegend). NK cell proliferation was analyzed by labeling cells with 5 μM Cell Trace Violet (CTV, Thermofisher) before transfer, and CTV labeling was performed according to manufacturer protocol.

Ex vivo stimulation of Lymphocytes

Approximately 10^6 spleen lymphocytes were stimulated for 4 hr in RPMI containing 10% fetal bovine serum with 20 ng/mL recombinant mouse IL-12 (R&D Systems) plus 10 ng/mL IL-18 (MBL) or 50 ng/mL PMA (Sigma) plus 500 ng/mL Ionomycin (Sigma). Cells were cultured in media alone as a negative control.

Ex vivo killing assay

To test the cytotoxic capacity of *Irf9*$^{-/-}$ NK cells, Ba/F3 target cells and Ba/F3-m157 control cells were labeled differentially with Cell Trace Violet (CTV, Invitrogen), according to manufacturer protocol (Ba/F3, CTV^{lo}; Ba/F3-m157, CTV^{hi}). 5 × 10^3 of each cell line were mixed with 5 × 10^4 purified NK cells from WT or *Irf9*$^{-/-}$ mice, or without NK cells (control condition). Effector and target cells were co-cultured for 6 hours at 37°C in RPMI-1640 containing 10% FBS. After 6 hours, cells were stained with propidium iodide prior to flow cytometry. Percentages of target cell killing were determined using the following formula (adapted from (Viant et al., 2017)): 100 - ([(% Ba/F3-m157 cells/% Ba/F3 cells)]/[(% Ba/F3-m157 cells/% Ba/F3 cells) control] × 100). For this formula, only CTV$^+$ cells within live cells were considered. Percentage of PI$^+$ target and control cells was determined from total CTV^{hi} and CTV^{lo} cells respectively.

To test the ability of activated WT NK cells to directly kill *Irf9*$^{-/-}$ NK cells, NK cells were first enriched from spleens of pooled WT or *Irf9*$^{-/-}$ mice by negative selection over BioMag goat anti-rat IgG beads (QIAGEN) coated with rat anti-mouse CD8α, CD4, CD19, and Ter-119 antibodies (Bio X Cell, clones 2.43, GK1.5, 1D3, and TER-199 respectively). Enriched CD45.1$^+$CD45.2$^+$ WT NK cells were used as effectors cells against a 1:1 mix of CD45.1$^+$ WT and CD45.2$^+$ *Irf9*$^{-/-}$ NK cell targets. Effector and target cells were co-cultured for 16 hours at 37°C in RPMI-1640 containing 10% FBS and IL-2 (10 ng/mL), IL-12 (100 ng/mL), IL-18 (10 ng/mL), and IFN-α (100U/mL). After 16 hours, cells were stained with Annexin V and Fixable Viability Dye (eBioscience) prior to flow cytometry; double positive cells were considered dead.

RNA Sequencing

To determine the transcriptome of NK cells following stimulation with IFN-α, NK cells (TCRβ$^-$CD19$^-$CD3ε$^-$F4/80$^-$NK1.1$^+$CD49b$^+$) were sorted from C57BL/6 mice, incubated overnight with 100 U/mL IFN-α or no cytokine (unstimulated), then 5-8 × 10^4 NK cells were sorted again for purity. To determine the STAT1-, IFNAR1- and IRF9-dependent transcriptional events in NK cells during MCMV infection, 1.5-10 × 10^4 Ly49H$^+$ NK cells (TCRβ$^-$CD19$^-$CD3ε$^-$F4/80$^-$NK1.1$^+$Ly49H$^+$) were sorted from spleens of individual mBMC mice harboring WT (CD45.1) and IFN signaling-deficient (CD45.2) cells at d0, d2 or d4 PI with MCMV. RNA was isolated from sorted cell populations using TRIzol (Invitrogen) and total RNA was amplified using the SMART-seq V4 Ultra Low Input RNA kit (Clontech). Subsequently, 10 ng of amplified cDNA was used to prepare Illumina HiSeq libraries with the Kapa DNA library preparation chemistry (Kapa Biosystems) using 8 cycles of PCR. Samples were barcoded and run on Hiseq 2500 1T, in a 50bp/50bp paired-end run, using the TruSeq SBS Kit v3 (Illumina).

Chromatin immunoprecipitation and DNA sequencing

5-10 × 10^6 NK cells (TCRβ$^-$CD19$^-$CD3ε$^-$F4/80$^-$NK1.1$^+$CD49b$^+$) were sorted from spleens of pooled C57BL/6 mice and incubated overnight (16-18 hours) with cytokines. NK cells were stimulated with 100 U/mL IFN-α with or without 10 ng/mL IL-2. DNA and proteins were cross-linked for 8 minutes using 1% formaldehyde. ChIP was performed as previously described (Beaulieu et al., 2014; Zheng et al., 2007), using 10 μg of rabbit polyclonal anti-STAT1 antibody (Santa Cruz, sc-592, clone M-22), or 10 μg of rabbit polyclonal anti-IRF9 antibody (Santa Cruz, sc-496, clone C-20) followed by Illumina next-generation sequencing. Fragments between 100 and 600 bp were size selected and Illumina HiSeq libraries were prepared using the Kapa DNA library preparation chemistry (Kapa Biosystems) and 12-15 cycles of PCR. Adaptors were diluted 1/10 or 1/50 depending on the starting amount of material available. Barcoded libraries were run on Hiseq 2500 1T in a 50bp/50bp paired-end run, using the TruSeq SBS Kit v3 (Illumina). STAT1-ChIP was performed twice, while IRF9-ChIP was performed 3 times.

QUANTIFICATION AND STATISTICAL ANALYSIS

RNA-Seq Analysis

Paired-end reads were trimmed for adaptors and removal of low quality reads using Trimmomatic (v.0.36)(Bolger et al., 2014). Trimmed reads were mapped to the *Mus musculus* genome (mm10 assembly) using Bowtie2 (v2.2.9)(Langmead and Salzberg, 2012). Read counts overlapping exons according to the UCSC Known Gene model were generated using the summarizeOverlaps function from the GenomicAlignments package (v1.10.1)(Lawrence et al., 2013). Differential analyses were executed with DESeq2 (v1.14.1)(Love et al., 2014). Genes were considered differentially expressed if they showed an FDR adjusted p value < 0.05, adjusted for multiple hypothesis correction as calculated by the DESeq2 software. For gene set enrichment analysis, differentially expressed genes were passed into goseq (v1.32.0) using the PANTHER and REACTOME databases. Top pathways were ranked by p-value, selected only from those passing a threshold of FDR-corrected p < 0.05.

ChIP-Seq analysis and peak annotation

For STAT1-ChIP, paired-end reads were trimmed for adaptors and removal of low quality reads using Trimmomatic (v.0.36)(Bolger et al., 2014). Trimmed reads were mapped to the *Mus musculus* genome (mm10 assembly) using Bowtie2 (v2.2.9)(Langmead and Salzberg, 2012). Concordantly aligned paired mates were used for individual peak calling and pooled replicate peak calling by MACS2 (v2.1.1.20160309)(Zhang et al., 2008) with the arguments "-p 1e-2 -m 2 50 –to-large." Irreproducible discovery rate (IDR)(Li et al., 2011) calculations using scripts provided by the ENCODE project (https://www.encodeproject.org/software/idr/; v2.0.2 and v2.0.3) were performed on all pairs of individual replicate peak lists against the oracle peak list of pooled replicates. Reproducible peaks were thresholded for those showing an IDR value of 0.05 or less and used for further analysis. Peak assignment to genes and gene features was performed using ChipPeakAnno(Zhu et al., 2010). Promoter peaks were defined as peaks that overlapped a region that was +2kb to −0.5kb from the transcriptional start site (TSS). Intragenic (intronic and exonic) peaks were defined as any peak that overlapped with annotated intronic and exonic regions, respectively, based on the UCSC Known Gene annotation database(Speir et al., 2016). Intergenic peaks were defined as any non-promoter or non-intragenic peaks, and were assigned to the gene of the nearest TSS based on the distance from the start of the peak. Priority was given to transcripts that were canonical, based on the UCSC Known Canonical database.

For IRF9-ChIP, paired-end reads were mapped to the *Mus musculus* genome (mm10 assembly) using Bowtie2 (v2.3.2) with parameters –no-unal -X 500 –no-mixed –no-discordant. Concordantly aligned paired mates were used for individual peak calling and pooled replicate peak calling by MACS2 with the arguments "–nomodel –shift 100 –extsize 200 -p 0.2 -B –mfold 3 50 –SPMR –keep-dup 'auto'." IDR was calculated using custom bash scripts on all pairs of individual replicate peak lists against the oracle peak list of pooled replicates. Reproducible peaks were thresholded for those showing IDR < 0.01 and used for further analysis.

Gene tracks were generated by converting BAM files to bigWig files using bedtools2 (v.2.26.0)(Quinlan and Hall, 2010) and UCSC's bedGraphToBigWig (v.4)(Kent et al., 2010) and visualized using the Gviz R package (v.1.18.2)(Hahne and Ivanek, 2016).

Statistical Analyses

For graphs, data are shown as mean ± SEM, and unless otherwise indicated, statistical differences were evaluated using a two-tailed unpaired Student's t test, and Welch's correction. Statistical differences in survival were determined by Gehan-Breslow-Wilcoxon Test analysis. For RNA-seq data, significance cutoff was determined using multiple hypothesis corrected p values as calculated by DESeq2. $p < 0.05$ was considered significant and is indicated in figures by an "*." Graphs were produced and statistical analyses were performed using GraphPad Prism.

DATA AND SOFTWARE AVAILABILITY

The accession number for all RNA-seq and ChIP-seq data reported in this paper is GEO: GSE106139.